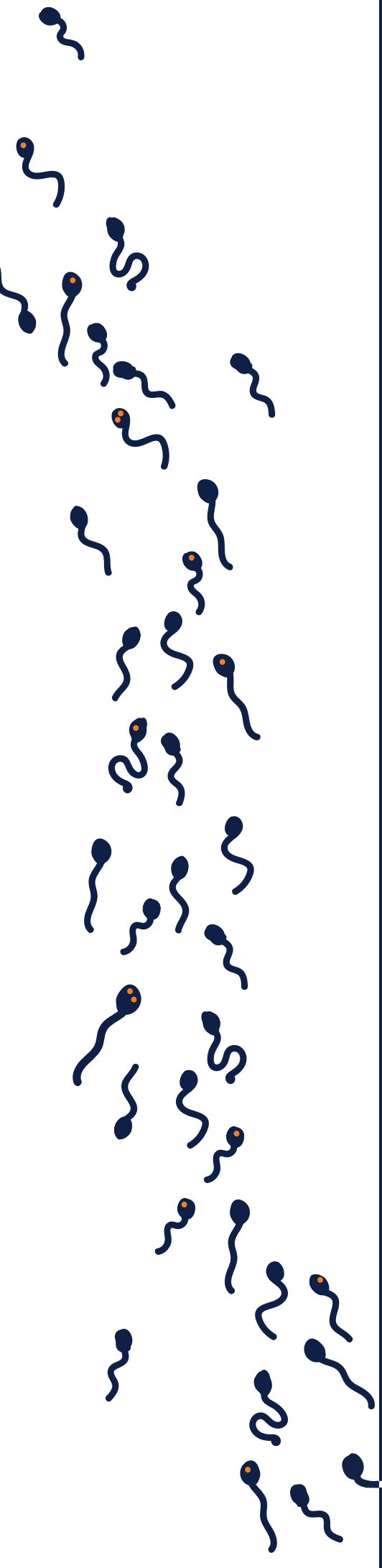

Localization and Planar Control of Nanoparticle-Coated Sperm Cells In Vitro

Iris Mulder

Faculty of Engineering Technology
Department of Biomedial Engineering

Examination committee
Dr. I. S. M. Khalil
Dr. J. Dasdemir
Dr. D. Wasserberg

January 2024

UNIVERSITY OF TWENTE.

Localization and Planar Control of Nanoparticle-Coated Sperm Cells *In Vitro*

Iris Mulder

***Abstract*— IRONSperm has remarkable potential to be used in the medical field for targeted drug delivery and assisted fertilization. Previous research has focused on characterization and one-dimensional movement of these microrobots, utilizing a stationary RPM. The aim of this study is to assess the feasibility of planar locomotion control, both in an unbounded environment and within a trifurcation phantom. Trials in an unbounded environment have demonstrated the importance of correct alignment of the RPM with respect to the cluster's confinement. Additionally, manual control of the RPM was found to have a positive effect on following the predefined trajectories more closely, particularly during joint movements. A proof of principle was established of successfully navigating a 3 mg/mL IRONSperm cluster to the left, straight and right branch in a trifurcation phantom with success rates of 64.2%, 58.3%, and 34.6%, respectively. Locomotion control has also proven possible towards the right and left fallopian tube in a real-size phantom of the female reproductive tract. The clusters have been visualized utilizing X-Ray. More research should be carried out to improve the accuracy of locomotion control and to investigate IRONSperm locomotion when facing differently structured surfaces and environments.**

I. INTRODUCTION

Chemotherapy is widely used as a treatment for various types of cancers. However, upon entering the body, it not only targets the intended tumorous site but it also interferes with all rapidly dividing cells, resulting in the destruction of healthy tissues [1]. In fact, most drugs that exhibit harmful side effects do so primarily due to the lack of mechanisms for targeted delivery to desired therapeutic sites, as the majority of drugs do not possess a natural affinity for their intended targets in the body [2].

To achieve precise and local drug administration in the body, drugs can be coupled to or encapsulated in a carrier, optimizing their delivery to selected cell types and phenotypes. These carriers can be introduced into the body through various pharmacological routes and have the capability to reach diverse organs and therapeutic targets [2].

A. Microrobots

Microrobots represent a type of carrier that holds significant potential for a multitude of biomedical *in vivo* applications, including remote-controlled drug and cell delivery, and minimally invasive surgery [3] [4]. Due to their small size and wireless control, microrobots present an alternative to catheter-based approaches, offering advantages such as decreased pain, reduced risk of infection, and minimized trauma [3][5]. Microrobots measuring only a few millimeters or less could enable surgeons to explore and treat hard-to-reach locations in the human body consisting of fluid-filled lumens, such as tubes and cavities, as well as soft tissues [5]. Instances of these locations include the circulatory system, the urinary system, and the uterus [4]. The capacity of untethered microrobots to navigate these anatomical locations is promising [6]. However, there are still some challenges that need to be researched and addressed before their widespread application in the medical field. Examples of such challenges include remote actuation, non-invasive localization and biocompatibility, and it is crucial to consider and quantify their trade-offs [7].

B. Magnetic actuation

One of the emerging methods to actuate microrobots *in vivo* is the use of magnetic fields. Magnetism on this scale is harmless, making it bio-compatible. Additionally, it enables remote long-range actuation and it undergoes little distortion or attenuation in the body [3] [7]. Furthermore, the magnetic gradient can apply sufficient force and torque to microrobots, enabling six-degrees-of-freedom motion [8] [9].

C. IRONSperm

Spermatozoa serve as an excellent template for such magnetically actuated microrobots, due to their intrinsic flexibility and drug loading capability. Owing to their organic components, they have low cytotoxicity. Coating the spermatozoa with magnetic nanoparticles enables magnetic actuation and provides a way to visualize the clusters *in vivo* using either X-rays or ultrasound [10]. A suspension of dead bovine sperm and iron nanoparticles can self-assemble into IRONSperm, because of the electrostatic forces between the negatively charged sperm cell membrane and the positively charged nanoparticles. This process is shown in Figure 1(A) [11]. Individual IRONSperm cells are able to swim through bulk fluids under the influence of a rotating permanent magnet (RPM). However, localizing and visualizing a single IRONSperm cell *in vivo* poses challenges due to its limited spatial resolution and the low contrast-to-noise ratio. Additionally, single cells are limited in their capacity to transport large quantities of drugs. To achieve better therapeutic results, researchers are looking into the collective behavior of IRONSperm by conducting tests on clusters of these microrobots [7].

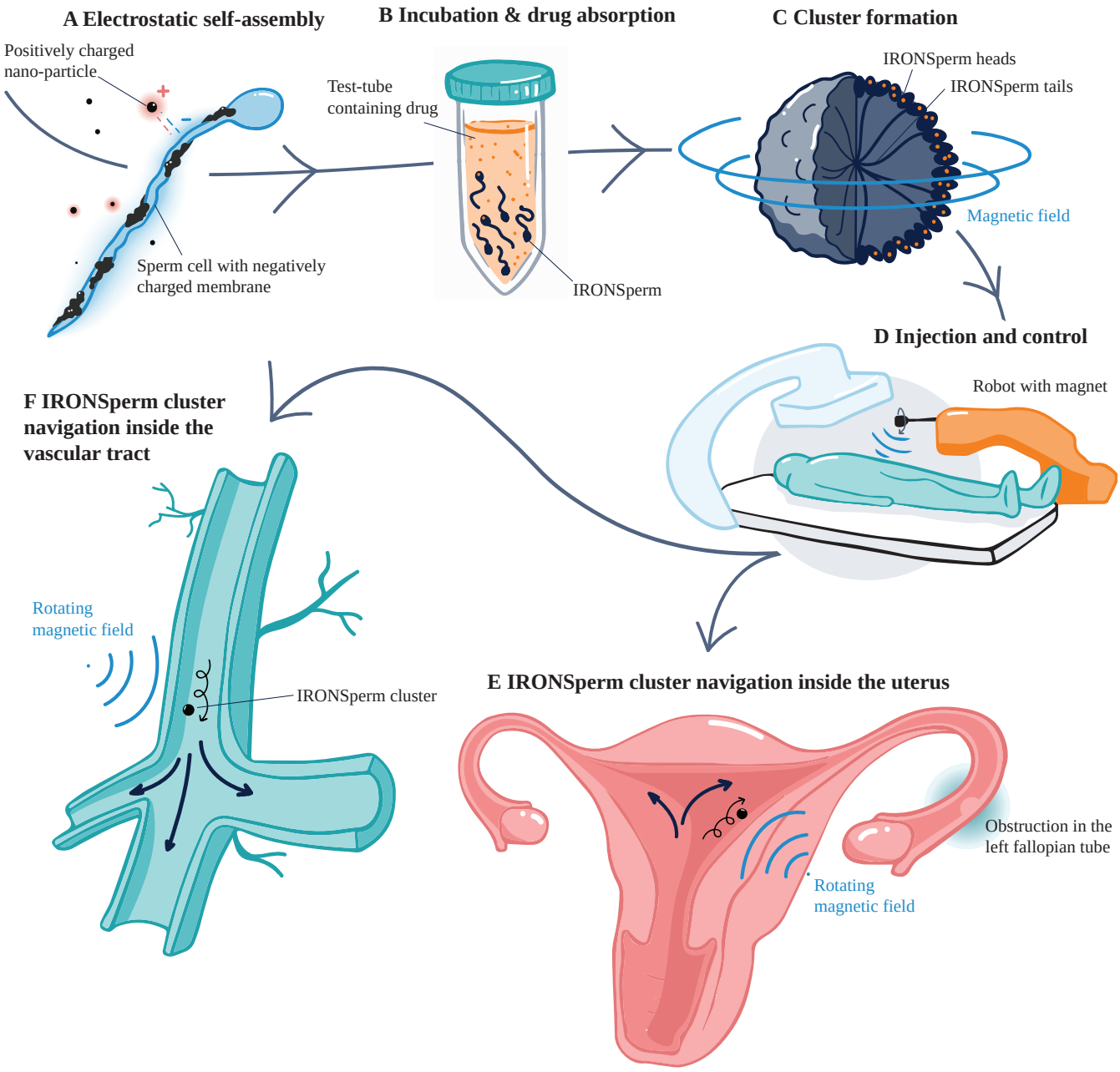

Fig. 1. **Fabrication of a drug-loaded IRONSperm cluster with examples of *in vivo* applications.**
(A) Positively charged nanoparticles undergo self-assembly onto the negatively charged sperm cell membrane, primarily concentrated at the tail. Once the sperm cell is fully coated, it assumes a black appearance and is referred to as 'IRONSperm.' **(B)** During the incubation of the IRONSperm, the drug is predominantly absorbed by the IRONSperm heads. **(C)** Utilizing an external magnetic field, the IRONSperm cells are collected and form a cluster. The heads and tails naturally orient outward and inward, respectively, creating a rigid structure due to remanence magnetization and entanglement [7]. **(D, E, F)** One or multiple clusters could be injected into the patient and could be navigated, for instance, inside the uterus or the circulatory tract. In these anatomical regions, the cluster encounters multiple possible pathways. This underlines the importance of understanding how to accurately control locomotion of IRONSperm clusters in the desired direction.

The IRONSperm clusters are created through entanglement, as well as electrostatic and magnetic self-assembly, see Figure 1(C) [11]. Research indicates that the magnetic material is agglomerated more in the center of the cluster, whereas the cell heads orient towards cluster's outer area. This holds great potential benefits for targeted drug administration [7]. The resulting connections are robust enough that the clusters can be considered as rigid structures [7].

D. Locomotion

When a magnetic field is applied, IRONSperm clusters will attempt to align their own preferred magnetization axis with the field [7]. In case of a rotating permanent magnet, the clusters will mimic its motion, causing them to roll along a nearby surface and effectively trailing on the RPM. This allows for a new form of actuation, called rolling locomotion [12].

Rolling locomotion is influenced by different factors, such as the rotation frequency of the RPM, the nanoparticle concentration and the size of the cluster. For low RPM frequencies, the angular velocity of the IRONSperm clusters is equal to the angular velocity of the magnetic field. However, above a certain 'step-out' frequency, the clusters oscillate and start slipping on the surface, resulting in a decrease of their average translational velocity [7] [13].

E. Physical interactions

In low Reynolds number environments, similar to the settings *in vivo*, the rolling locomotion of IRONSperm clusters is influenced by several physical interactions. Firstly, magnetic fields and gradients can exert forces and torques on microrobots, enabling six degrees of freedom [7]. This magnetic torque (τ_m) is dependent on the dipole moment (m) and the magnetic field strength (B), such that: [10]

$$\tau_m = m \times B. \tag{1}$$

The magnetic torque counterbalances the drag torque in the medium. The viscous drag torque is defined as: [10]

$$\tau_d = f_r \times \omega_c, \tag{2}$$

where f_r is the rotational drag coefficient of the cluster and ω_c is its angular velocity [10].

Finally, a torque denoted as τ_s, is exerted on the cluster due to the friction forces resulting from contact with the surface. This torque is significantly smaller for rolling motion compared to sliding motion across all size scales. This presents another advantage of using IRONSperm clusters instead of individual IRONSperm cells [14].

The forces on a magnetic roller are balanced as: [15]

$$\tau_m + \tau_d + \tau_s = 0. \tag{3}$$

F. Objective

Swarms of magneto-tactic bacteria have been successfully steered through vascular structures [16]. This raises the question whether this is also possible for IRONSperm microrobots.

Thus far, research reveals that a stationary RPM can enable IRONSperm clusters to roll back and forth in one-dimension, covering distances in the order of centimeters. To expand the potential applications of IRONSperm to the human body, it is important to identify whether IRONSperm clusters are able to cover larger distances and to understand how to navigate a cluster through complex networks, branches and bifurcations, similar to those found *in vivo*. Consequently, further investigation is required to comprehend planar IRONSperm cluster guidance and locomotion.

The objective of this study is to examine the feasibility and precision of planar IRONSperm locomotion control by evaluating its capability to follow a predefined trajectory at a set speed and RPM. This investigation will be conducted both in an unbounded environment and within a trifurcation phantom, featuring cylindrical branches enclosed on all sides. The aim is to establish a proof of principle of locomotion control within the trifurcation phantom in each branch. The impact of confinement on the cluster's ability to effectively follow the trajectory will be investigated. Finally, the feasibility of obtaining real-time visual feedback is evaluated through an experiment conducted with a 3 mg/L IRONSperm cluster placed inside both the trifurcation phantom and an anatomically accurate, real-size phantom of the female reproductive tract.

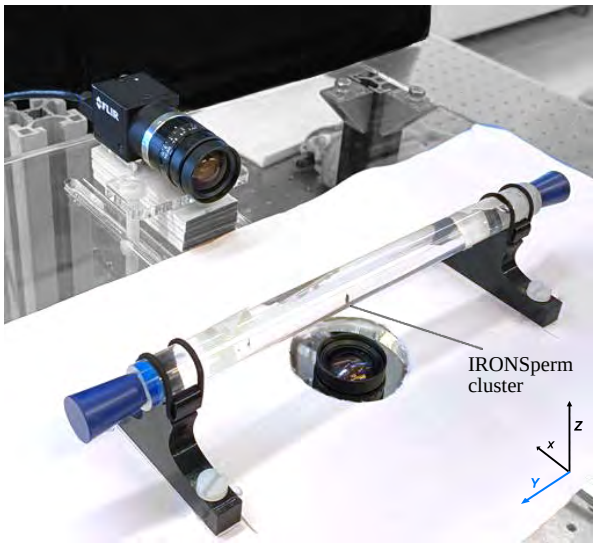

Fig. 2. Top view of the set-up of Experiment 1. A 3 mg/L IRONSperm cluster is actuated using a rotating magnetic field about the x-axis, which is not shown in frame. This yields rolling along the y-axis.

II. METHODOLOGY

A. Sample fabrication

Nanoparticle-coated bull sperm cells were fabricated by electrostatic-based self-assembly [7]. 500 µL suspension of 2.5×10^7 sperm cells/mL and 150 µL iron oxide (Fe_3O_4) nanoparticle solution of 10 mg/mL were added to a micro-centrifugation tube, resulting in a nanoparticle concentration of 3mg/mL [17].

Among various nanoparticle concentrations (1 mg/mL, 2 mg/mL and 3 mg/mL), it was decided to conduct experiments with 3 mg/L concentration clusters, as they are hypothesized to have stronger interactions with the external magnetic field and have a higher contrast to noise ratio when using medical imaging [13]

B. Experiment 1: Determining the optimal RPM speed for linear movements

In prior research involving rolling locomotion of IRONSperm clusters, the RPM frequency underwent variations while maintaining a stationary position. To investigate the potential of an IRONSperm cluster to trial on a predetermined path, it is necessary to establish the cluster's ability to track a moving RPM. This involves determining the speeds at which such synchronization is feasible. The objective of Experiment 1 is to investigate the optimal linear speed of the RPM in one-dimensional movements for which the cluster can effectively maintain synchronization. The experimental set-up is illustrated in Figure 2.

The cluster is placed within a transparent acrylic tube, with an inner diameter of 10 mm and an outer diameter of 15 mm, and immersed in 0.9% saline solution. Adhering to previous research, the RPM of the external permanent

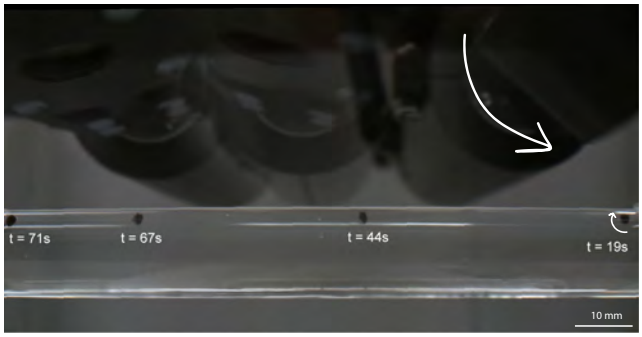

Fig. 3. Visualization of the linear movement of the IRONSperm cluster with respect to the RPM over time.

magnet is set below the step-out frequency, precisely at 1.5 Hz [13]. The external magnet is cylindrical (NdFeB Grade-N45) with a height of 20.0 mm and a radius of 17.5 mm. The clusters receive a maximum magnetic field strength of 28 mT. The separation distance between the center of the magnet and top of the tube is maintained at 50 mm, as previously demonstrated to be viable [13]. It is important to note that the test conditions were highly specific. As a result, the findings of this experiment may not be widely applicable to IRONSperm research under different conditions.

The robot moves linearly across a span of 110 mm with various speeds, ranging from 4 mm/s to 10 mm/s. Before each trial the RPM direction is altered several times to verify magnetic coupling with the cluster. The motion of the cluster in response to the magnet movement is recorded at a rate of 30 frames per second, using a FLIR Blackfly camera equipped with a Fujinon 1:1.2/6 mm lens. Both forward and backward movements are investigated by altering the direction of the RPM and adjusting the direction of the movement of the robot.

C. Experiment 2: Synchronizing with predefined paths in an unbounded environment

Experiment 2 is structured to investigate the planar IRONSperm cluster locomotion in an unbounded environment at the optimal speed identified in Experiment 1, while following trajectories that will later be utilized in a trifurcation phantom in Experiment 3. To achieve this, a transparent plastic box filled with saline solution was utilized, as depicted in Figure 5. The inner diameter of the box measures 11 mm, with a thickness of 4 mm, resulting in a total height of 19 mm. The RPM and magnet to cluster distance were kept consistent to Experiment 1. The camera was placed below the box. The predefined right, straight and left trajectories, see Figure 18(B-D), are transferred to an industrial KUKA robotic arm through a Python script and the program 'RoboDK'. These tools facilitate the translation of trajectory drawings into multiple small targets that the robot will move between.

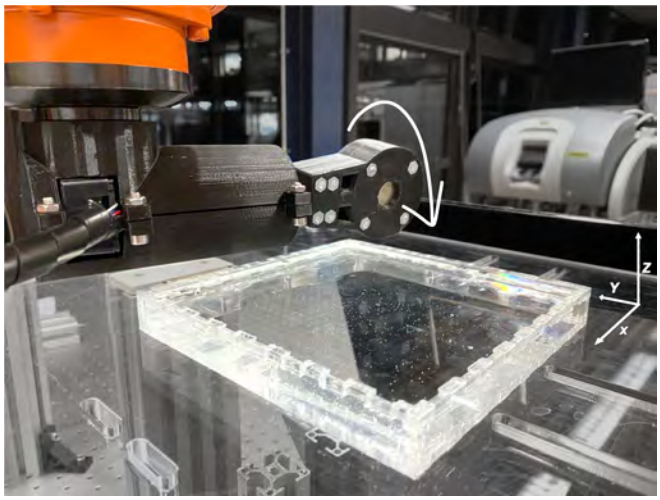

Fig. 4. Set-up of Experiment 2

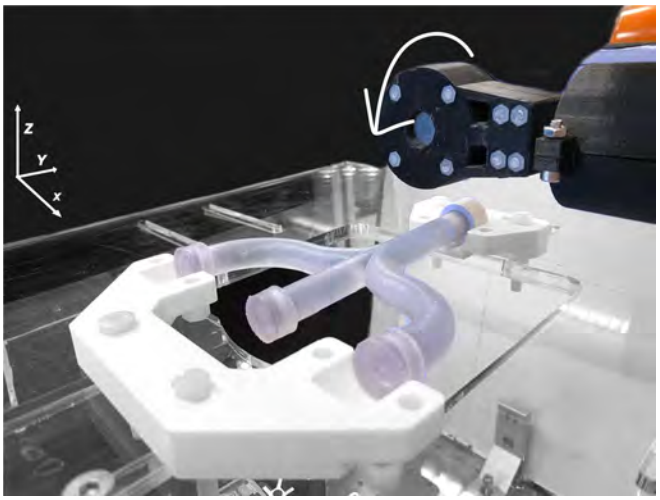

Fig. 5. Set-up of Experiment 3

Initially, the trajectories and RPM were actuated fully automatically by the robot, to enhance the replicability of the experiment. However, through trial and error it was discovered that the cluster's proximity to the RPM could be controlled by manually altering the direction of the RPM, inducing back-and-forth movement around the same spot. This could potentially improve the cluster's ability to closely follow the intended trajectory. This was also tested during Experiment 2.

D. Experiment 3: Synchronizing with predefined paths in the trifurcation phantom

The objective of Experiment 3 is to assess locomotion control in various directions in an enclosed environment at the optimal speed identified in Experiment 1. This would give more insight on the impact of confinement on guiding the cluster along the intended path. To achieve this, a trifurcation phantom is used, filled with a 0.9% saline solution. The phantom is designed to mimic branching in the vascular system, featuring three distinct cylindrical branches that enclose the cluster on all sides. Each branch has an outer diameter of 15 mm and the entire phantom measures 140 mm by 125 mm. The aim of this experiment is to establish a proof of principle demonstrating successful navigation of a cluster towards the right, straight and left branch.

The experimental set-up is visualized in Figure III-C. The RPM and the distance between the magnet and the cluster were consistent with those in used Experiment 1. The FLIR Blackfly camera is positioned beneath the pitchfork, in order to capture and visualize the two-dimensional movement.

Once again, both the forward and backward movements of the cluster are examined by altering the RPM and the robot path direction.

E. Data processing

The recordings were analyzed using a MATLAB script that tracks the cluster's position over time. This script is detailed in Section VI-A.

III. EXPERIMENTAL RESULTS

A. Experiment 1

The cluster's velocity was examined under the influence of eight different linear robotic arm speeds, namely 4 mm/s, 5 mm/s, 6 mm/s, 6.5 mm/s, 7 mm/s, 7.5 mm/s, 8 mm/s, and 10 mm/s. Each trial was recorded at least four times (twice backward and twice forward). For each speed, trial results were combined into a mean with standard deviation, as depicted in Figure 6. The plot illustrates the cluster's X-position over time. Certain lines in the plot are concluded prematurely, indicating that the cluster lost magnetic coupling during the trials and failed to reach the other end of the acrylic tube.

Figure 16 provides a more detailed visualization of the cluster's locomotion in response to different robot speeds. The rolling movement of the cluster is particularly well-illustrated in Figure 16, depicted by the sinusoidal shape in the plots. The loss of magnetic coupling is visually represented by the cluster descending to the bottom of the acrylic tube.

Results indicated that the cluster followed the magnet successfully at speeds ranging from 4 to 7 mm/s. At speeds of 8 and 10 mm/s, the cluster consistently lost magnetic coupling. The speed of 7.5 mm/s exhibited varying outcomes in terms of successful magnetic coupling. Every trial conducted at a robot speed of 7 mm/s was considered successful, leading to the selection of this speed as the optimal choice for all subsequent Experiments. In Section 16, a more in-depth analysis of these results will be conducted.

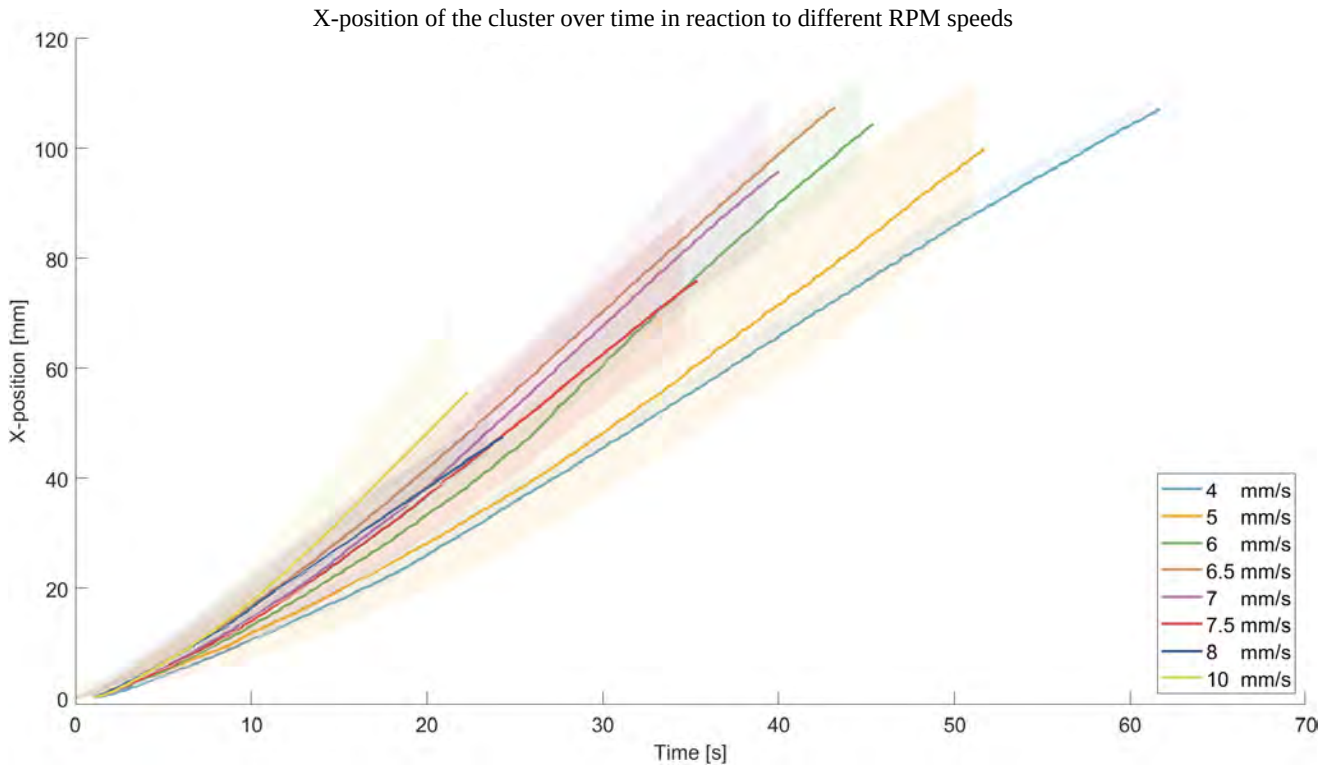

Fig. 6. X-position of the IRONSperm cluster over time in response to different linear speeds of the external magnetic field. The presented plot illustrates the mean and standard deviation (STD) values derived from a minimum of four trials conducted at each speed.

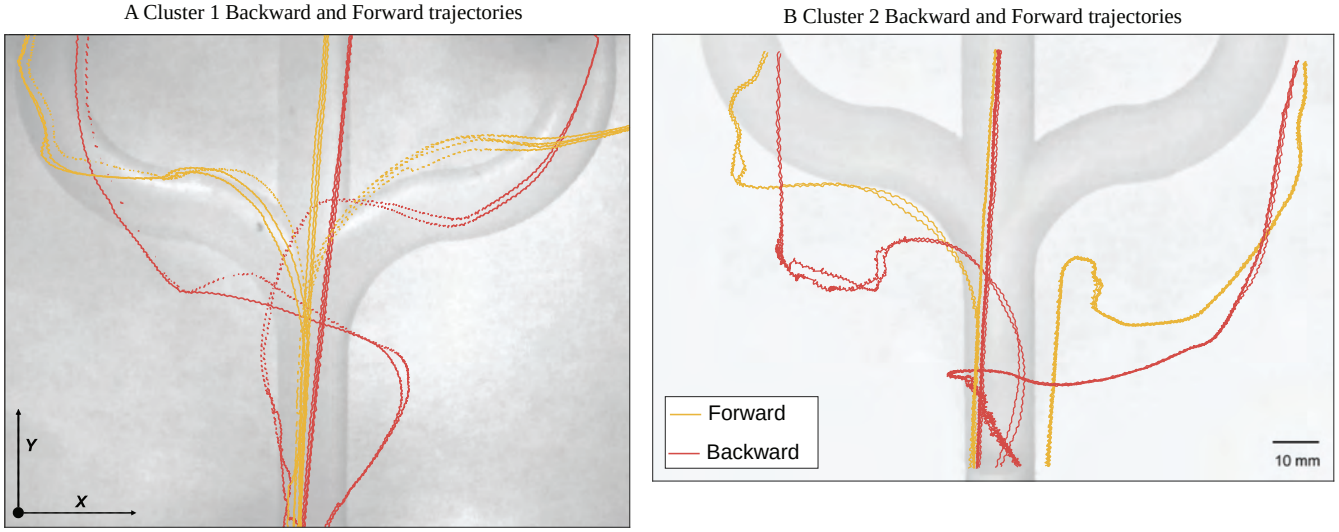

Fig. 7. Visualization of two distinct clusters of 3 mg/mL following the same trajectories on different days. Forward and backward paths are depicted with the yellow and red plots, respectively. For contrast, the outlines of the trifurcation phantom are added virtually.

B. Experiment 2

Experiment 2 investigated planar IRONSperm cluster locomotion in a non-enclosed environment, exploring both forward and backward motion along trifurcation trajectories. The study also examined the influence of manual versus automatic RPM control. The resulting cluster paths are visualized in Figures 8 and 7. Visual phantom outlines in the images demonstrate whether the cluster would have remained within the confinement. While most paths showed minimal deviation, Figure 8C, 8D and 8E revealed some divergence, which will be discussed in Section IV-C.

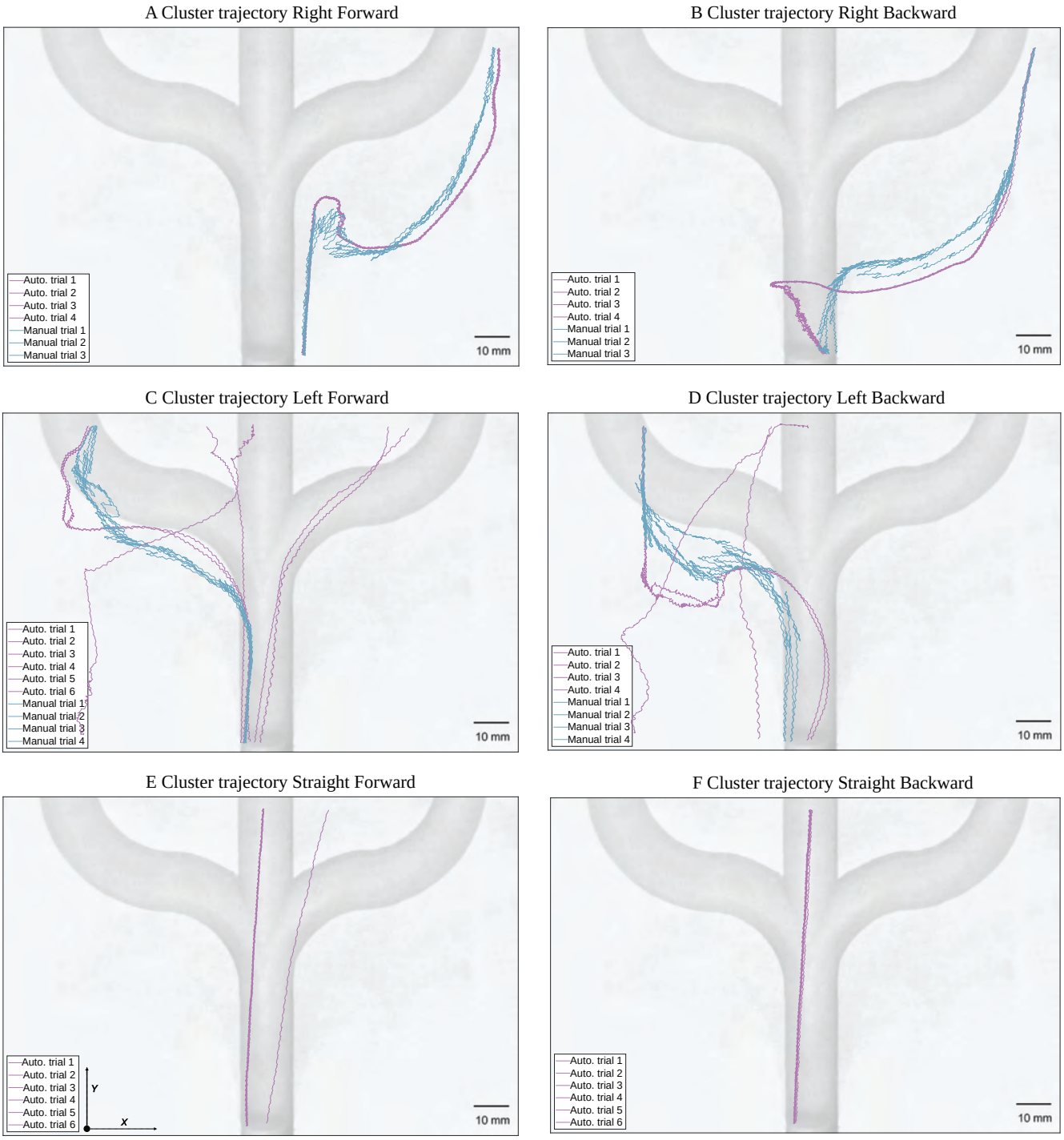

Fig. 8. Visualization of the travelled paths on the flat surface in each direction, both fully automatic (purple) and utilizing manual RPM intervention (blue). For contrast, the outlines of the trifurcation phantom are added virtually. Figures E and F exclusively present automatic trajectories, as manually controlling the RPM in the straight path did not contribute any value, given its absence of bends or joint movements.

C. *Experiment 3*

The objective of Experiment 3 was to establish a proof of principle, demonstrating that an IRONSperm cluster can be directed into the right, straight and left branch of the trifurcation phantom. A trial is considered successful if the cluster eventually rolls into the intended branch. A small deviation into another branch is allowed here. Moreover, the cluster is not required to reach the end of the branch; it only needs to navigate the trifurcation correctly. Further elaboration on this topic will be provided in Chapter IV-D. The 'failed' trials refer to instances where the cluster did not reach the intended branch but instead reached another

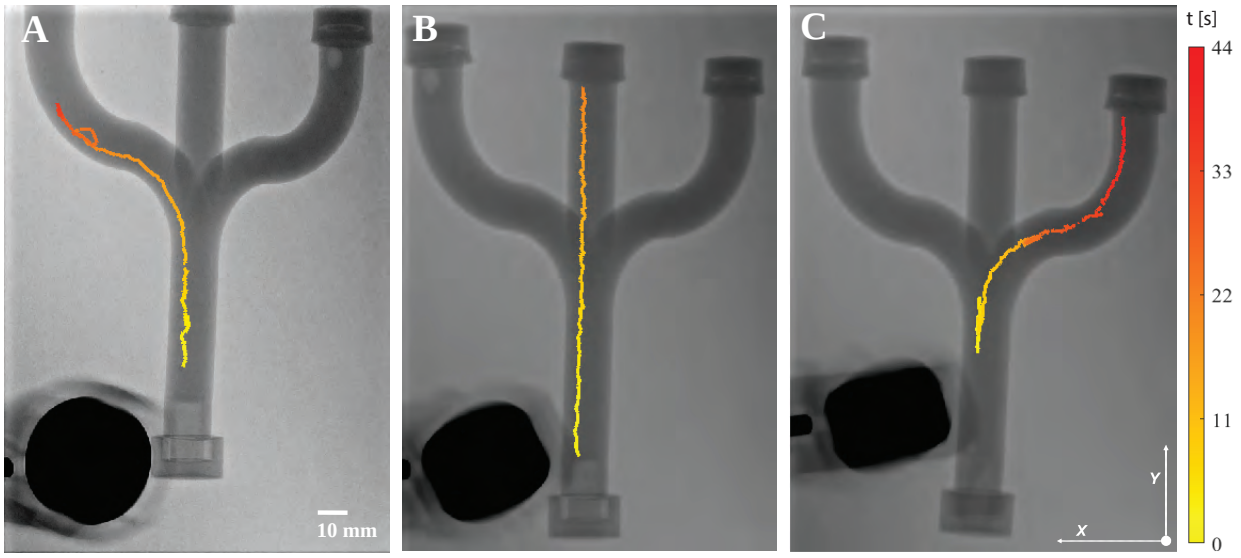

Fig. 9. Successful trials of the forward right, straight and left branch in the trifurcation phantom. The trajectory of the cluster is visualized over time [s], depicted by the color gradient line. Certain segments of the trajectory were not visible in the X-ray images due to the absorption of radiation by the RPM.

branch or remained in the backward branch. Trials deemed unsuccessful due to the cluster getting stuck or encountering other issues are not accounted for in this context.

Figure 9 illustrates the proof of principle of forward motion of the cluster into the right, straight and left branch recorded using X-Ray imaging. The trajectories of the travelled paths are visualized over time, indicated by the gradient line transitioning from red to yellow. The experiment was repeated multiple times, and the success rate of all recorded trials are shown in the histogram in Figure 10.

Out of all trials intended to roll into the right branch, 34.6% successfully reached their destination. The straight and left branch achieved success rates of 58.3% and 64.2%, respectively. Backward motion from each of the three branches into the main branch proved more successful, with a success rate of 75.0%.

D. Localization

To implement open-loop control during experiments with IRONSperm, it is important to devise a method to visualize the clusters. This becomes particularly valuable in non-transparent environments, such as *ex* or *in vivo* settings. Conducting CT scans both before and after each travelled trajectory enables researchers to confirm that the cluster initiated and concluded its movement at the intended positions.

The presence of nanoparticles within the clusters would allow for the application of X-ray and CT [10]. To validate this concept, an experiment was conducted involving a 3 mg/L IRONSperm cluster placed inside the trifurcation phantom and inside an anatomically accurate, real-size phantom of the female reproductive tract. The cluster was guided towards both the right and left fallopian tube using an external magnetic field and each trial was recorded using the FLIR Backfly camera and X-ray imaging. The experimental set-up is shown in Figure 17. Figure 11 illustrates the position of the cluster over time in the uterus phantom.

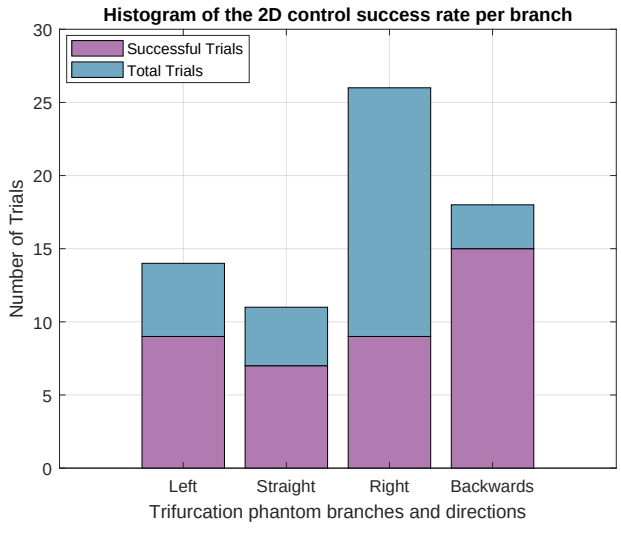

Fig. 10. Histogram depicting the distribution of successful and failed trials in the right, straight, left and backward branch. In the left branch, 9 out of 14 trials successfully reached the intended destination, while the straight path saw success in 7 out of 12 trials, the right branch in 9 out of 26 trials, and the backward direction in 15 out of 18 trials.

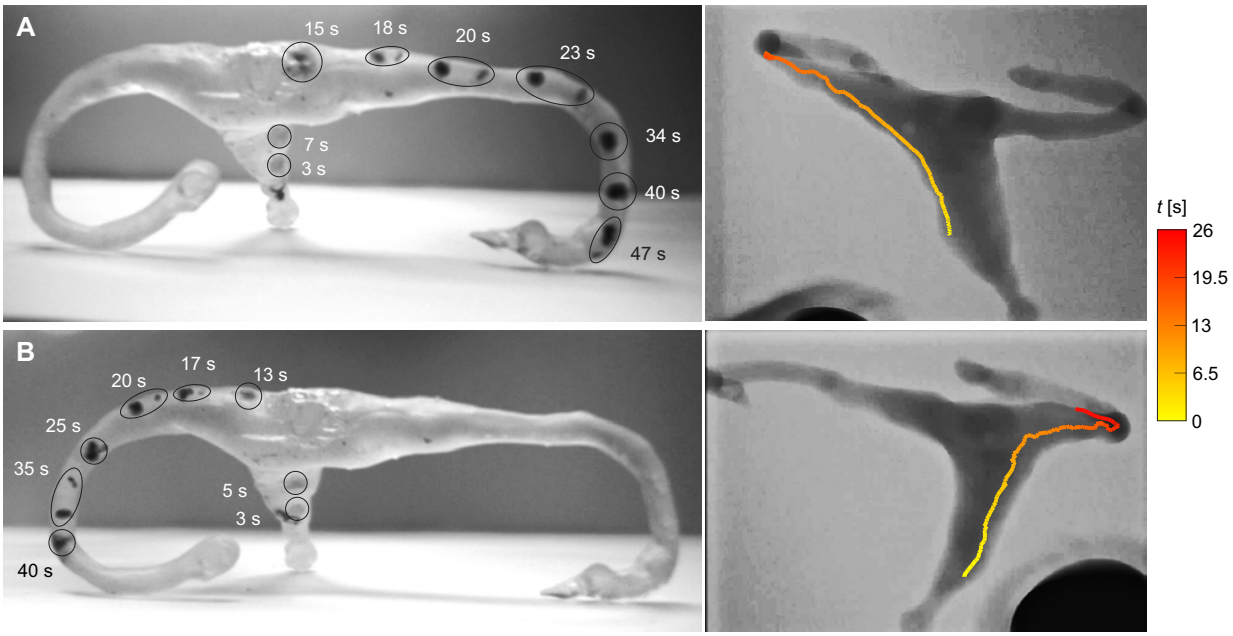

Fig. 11. Cluster position over time in the left **(A)** and right **(B)** fallopian tubes in a uterus phantom, recorded using a camera and X-ray. The ellipsoids highlight the cluster position over time. At certain instances, the cluster split up into multiple particles. In that case, all particles belonging to that timestamp are encircled together.

IV. DISCUSSION

A. Cluster velocity in response to different RPM speeds

The outcomes of Experiment 1 are presented in Figure 6, where the X-position of the cluster is plotted over time. Given that all trials were conducted at a consistent RPM frequency of 1.5 Hz and a notable discrepancy in cluster velocities is visible, it can be concluded that the magnetic gradient exerted a substantial influence on the cluster's velocity. Nevertheless, as the robot speed increases, the cluster will eventually lag behind due to friction and drag forces. As a result, trials at speeds of 7.5 mm/s, 8 mm/s, and 10 mm/s concluded prematurely due to a loss of magnetic coupling. This could be attributed to the drag torque, which scales linearly with the clusters velocity, as seen in Equation 2. The mean of the 7.5 mm/s trials indicates a lower cluster velocity than to be expected before experiencing magnetic decoupling, whereas the cluster's velocity in response to the highest tested robot speed (10 mm/s) remains the highest prior to magnetic decoupling. At a linear robot speed of 6.5 mm/s, an unexpected trend is observed once again, as the velocity of the cluster appears to be faster than that at 7 mm/s. This discrepancy could be attributed to the comparatively large STD of the 7 mm/s measurements, whereas the measurements at 6.5 mm/s demonstrate a higher level of consistency. In general, a significant STD can be observed between different trials of the same robot speed. These differences could be attributed to the cluster shape. This topic will be further elaborated in Section IV-B.

Ultimately, the robot speed of 7 mm/s was chosen for all subsequent experiments, as all trials conducted at this speed were considered successful. In a clinical setting, this would correspond to a cluster velocity of 0.23 body lengths per minute, calculated based on the average measurements of the Dutch male population [18].

B. Cluster properties

During this study, two distinct 3 mg/L clusters were utilized, assuming that the differences between them would be negligible. However, certain properties, such as the shape, might have an impact on locomotion. Figure 8E illustrates a trial in which the cluster deviated significantly from the straight-line path of the external magnetic field. This behavior might be attributed to the cone-like shape of the specific cluster during that trial, see Figure 15. Figure 8C and 8D also show trajectories that could be considered as "failed" trials. It seems the cluster rolls in exactly the opposite direction of the RPM. Additionally, Figure 7A and 7B depict an experimental iteration involving two distinct 3 mg/mL clusters on different test days showing significant deviations among them, specifically on the right trajectory. Furthermore, in the course of Experiment 1, it was noted that the shape of the cluster exerted a noteworthy influence on its velocity. Ellipsoidal shapes exhibited reduced speed, and other shapes introduced more slip, consequently leading to a decrease in the overall average speed. This characteristic is recognisable through the larger rotations exhibited by the cluster, as illustrated in Figure 16. Moreover, some clusters disintegrated into multiple particles. During trials, these particles occasionally collided or interacted with each other, influencing the results. It would be beneficial to explore different fabrication methods to prepare samples in a manner that maintains the cluster's rigidity and spherical shape. The

findings also suggest the need for further research on the impact of cluster shape on locomotion, although this may have less effect inside an enclosed environment.

C. KUKA Robot limitations

One of the most challenging aspects of trajectory planning was manually aligning the robot with the precise start position of the trifurcation phantom. An incorrect configuration of the start position had consequences for the rest of the trajectory. This is clearly visible in Figure 8, where the travelled paths resemble the trifurcation phantom's outlines closely, but are positioned incorrectly. The industrial KUKA robot, with its large workspace, was used for a relatively small workspace, making it difficult to achieve precision. This was also observed by Braks in previous research [19]. Therefore, a recommendation would be to consider utilizing a cobot. Cobots are characterized by a smaller workspace, finer precision in movements, and reduced risk for users, and may be more suitable for the purpose of this research [20].

Additionally, the KUKA robot distinguishes between linear and joint speeds. When transitioning between targets with a different orientation, the robot will engage in joint movements. While the linear speed was set at 7 mm/s, determining the precise speed of the joint movements presented a challenge. As long as the cluster can keep pace with the external magnetic field, the specific speed can be considered adequate for the purposes of this study. Nonetheless, it is important to acknowledge this when attempting to replicate the experiment.

Moreover, lower speeds observed during joint movements, have possible led to the large deviations of the cluster from the intended trajectory during the fully automatic trials, as seen in Figure 8A-D. At those instances, the robot remained nearly stationary. However, when the external magnet was still rotating during these movements, the cluster would continue to advance, as illustrated in previous research by Weber [13]. As a result, the cluster would precede the RPM, leading to deviations from the intended trajectory. This phenomenon could also explain the difference between the backward and forward trajectories, as depicted in Figure 7. Manual trials exhibited more similarity between the backward and forward paths compared to the fully automatic trials. Furthermore, trials with manual RPM intervention, despite often being misaligned with the phantom, showed greater resemblance to the predefined paths.

In the context of the trifurcation phantom, the automatic RPM frequently led the cluster to unintentionally reach the straight branch. This was the case for 47% of the failed trials. Figure 12 illustrates how a cluster was steered back to the right branch using RPM altering, after nearly deviating toward the straight branch. Changing the RPM direction also proved beneficial for navigating past obstacles in the phantom or freeing the cluster when stuck. In conclusion, it is advisable to investigate the advantages and disadvantages of manual RPM intervention and assess its feasibility in scenarios involving open-loop control.

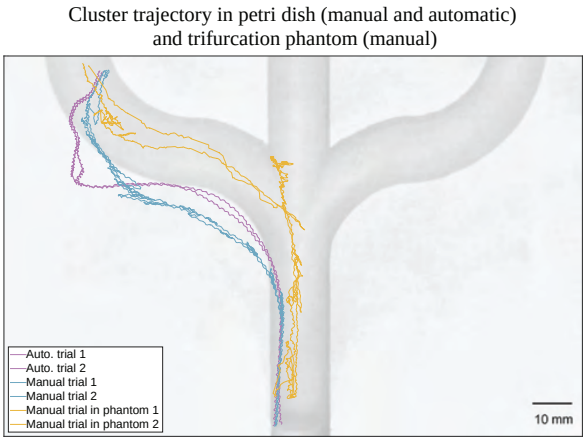

Fig. 12. Visualization of the travelled paths inside the trifurcation phantom (yellow) and on the flat surface, both fully automatic (purple) and utilizing manual RPM intervention (blue).

D. Trifurcation phantom

The success rate percentages found during Experiment 3 were derived from a relatively small sample size, and more extensive research is required in order to precisely assess the accuracy of planar locomotion control.

A significant portion of the unsuccessful trials was due to the cluster getting stuck inside the phantom, constituting 26.1% of recorded failures. The phantom's resin interior occasionally exhibited a sticky texture, causing the cluster to adhere to the boundary. Although the cluster remained visibly coupled to the magnetic field, it would not move any further. Internal 3D-printing supports within the left and right phantom branches, indicated in Figure 13, also posed challenges. The exact size of these supports is unknown, emphasizing the need to understand the cluster's ability to overcome obstacles of varying sizes. Since surfaces *in vivo* are not always smooth, it is recommended to conduct experiments with IRONSperm on various structures to gain more insights into this matter.

A potential solution to overcome obstacles that occasionally proved effective was to increase the distance between the RPM and the cluster. This adjustment reduced the cluster's attraction to RPM, thus allowing it to fall back slightly and move 'over' the obstacle. However, it is crucial to note that, as soon as the cluster reached the boundary on the other side, it would change locomotion direction and occasionally lose magnetic coupling completely.

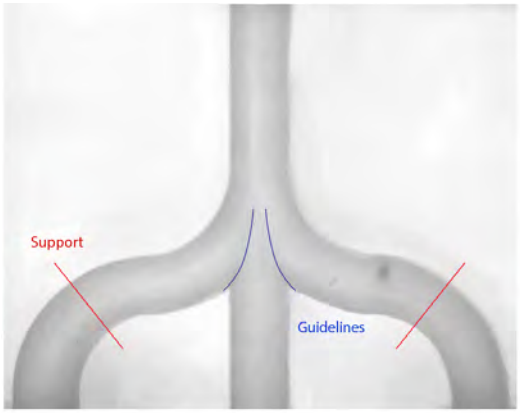

Fig. 13.

Additionally, the impact of confinement on the locomotion of the cluster is visualized in Figure 12. The Figure shows that the cluster is capable of synchronizing with the RPM within the trifurcation phantom, even though the RPM may have been misaligned, seeing that all trajectories on the flat surface exhibit considerable deviations from the phantom outlines. This observation underscores the cluster's ability to be guided in the correct direction by the confinement imposed by the phantom.

E. Trifurcation phantom vs. the circulatory tract

This research has demonstrated a proof of principle of controlling planar IRONSperm locomotion inside a trifurcation phantom. In this section, a comparison is made between the phantom and real-life scenarios to explore potential applications in vivo.

1) Viability in vivo: A good stability of the IRONSperm clusters in 10% fetal bovine serum was observed during cytotoxicity studies [7]. The biocompatibility of IRONSperm was tested by Magdanz on a human endometrial cell line. No increased number of dead cells was observed after 24 hours or 3 days, demonstrating the biocompatibility of IRONSperm and its potential for biomedical applications [10].

2) Bloodvessel characteristics: The experiments of this research have been conducted in a 0.9% saline solution with the viscosity and density equivalent to water, which are 1.0 mPa s and 997 kg/m³, respectively. These properties are similar to those of blood serum, which has a viscosity of 1.105 mPa s and a density of 906 kg/m³. Consequently, the hydrodynamic drag coefficients, drag forces, and torques are expected to be approximately similar in blood serum [7].

Bozuyuk et al. developed a model to investigate the locomotion of microcontrollers of various sizes in different segments of the vascular system. The results suggested that upstream locomotion of microrollers was entirely feasible in venous flow and partially achievable in arterial flow. However, locomotion was unsuccessful in smaller vessels such as venules, arterioles, and capillaries, primarily due to confinement and increasing flow effects [21]. The pulsating flow of blood that the microrobot encounters, is significant to a small, untethered device [5]. However, due to the parabolic flow profile, the flow along the vessel's walls is considerably lower than at the center. This characteristic could be advantageous for IRONSperm clusters, as they roll along the vessel walls, enabling them to evade strong fluidic effects. Additionally, low-density clusters potentially might let a portion of the flow pass through their body [21]. However, the presence of red blood cells introduces additional resistance and significantly influences the upstream locomotion of surface microrollers [5].

Even more resistance may be induced by the inner walls of blood vessels, characterized by packed endothelial cells that present surface microtopographies. These microtopographies significantly impede the locomotion of spherical surface microrollers [21]. As discussed in Section IV-D, a considerable part of the failed trials were attributed to the internal structure of the phantom. This raises the question whether IRONSperm clusters would be able to roll on vascular tract internal surface. More research should be conducted to determine locomotion control when facing different surfaces and environments, as well as testing the performance of IRONSperm clusters against different flow rates.

V. CONCLUSIONS

During this research a proof of principle was established of successfully navigating a 3 mg/mL IRONSperm cluster to the left, straight and right branch in a trifurcation phantom with success rates of 64.2%, 58.3%, and 34.6%, respectively. Locomotion control has also proven possible towards the right and left fallopian tube in a real-size phantom of the female reproductive tract. The clusters have been visualized utilizing X-Ray.

Trials on a flat surface have demonstrated the importance of correct alignment of the external magnetic field with respect to the confinement. However, even when the RPM is misaligned, the phantom's boundaries can play a significant role in guiding the cluster in the right direction nonetheless. Additionally, the impact of the automatic RPM operation was evident during certain robot joint movements, where the cluster exhibited unintended deviations. Manual control of the RPM was found to be beneficial, aiding in closely following the predefined trajectories.

References

References

[1] Won Duk Joo, Irene Visintin, and Gil Mor. *Targeted cancer therapy - Are the days of systemic chemotherapy numbered?* Dec. 2013. DOI: 10.1016/j.maturitas.2013.09.008.

[2] Vladimir Muzykantov and Silvia Muro. *Targeting delivery of drugs in the vascular system*. Tech. rep. Pennsylvania: Int J Transp Phenom., 2011, pp. 41–49.

[3] Sungwoong Jeon et al. *Magnetically actuated microrobots as a platform for stem cell transplantation*. Tech. rep. 2019. URL: https://www.science.org.

[4] Bradley J. Nelson, Ioannis K. Kaliakatsos, and Jake J. Abbott. *Microrobots for minimally invasive medicine*. Aug. 2010. DOI: 10.1146/annurev-bioeng-010510-103409.

[5] Yoichi Haga and Masayoshi Esashi. "Biomedical microsystems for minimally invasive diagnosis and treatment". In: *Proceedings of the IEEE*. Vol. 92. 1. Institute of Electrical and Electronics Engineers Inc., 2004, pp. 98–114. DOI: 10.1109/JPROC.2003.820545.

[6] Hakan Ceylan et al. *Translational prospects of untethered medical microrobots*. July 2019. DOI: 10.1088/2516-1091/ab22d5.

[7] Kaz I.N.A. Middelhoek et al. "Drug-Loaded IRONSperm clusters: Modeling, wireless actuation, and ultrasound imaging". In: *Biomedical Materials (Bristol)* 17.6 (Nov. 2022). ISSN: 1748605X. DOI: 10.1088/1748-605X/ac8b4b.

[8] Eric Diller et al. "Six-degree-of-freedom magnetic actuation for wireless microrobotics". In: *International Journal of Robotics Research* 35.1-3 (Jan. 2016), pp. 114–128. ISSN: 17413176. DOI: 10.1177/0278364915583539.

[9] Zhengxin Yang and Li Zhang. "Magnetic Actuation Systems for Miniature Robots: A Review". In: *Advanced Intelligent Systems* 2.9 (Sept. 2020). ISSN: 2640-4567. DOI: 10.1002/aisy.202000082.

[10] Veronika Magdanz et al. *IRONSperm: Sperm-templated soft magnetic microrobots*. Tech. rep. 2020, pp. 5855–5863. URL: https://www.science.org.

[11] Veronika Magdanz et al. "Sperm–Particle Interactions and Their Prospects for Charge Mapping". In: *Advanced Biosystems* 3.9 (Sept. 2019). ISSN: 23667478. DOI: 10.1002/adbi.201900061.

[12] Yu Zeng and Bin Liu. "Self-propelling and rolling of a sessile-motile aggregate of the bacterium Caulobacter crescentus". In: *Communications Biology* 3.1 (Dec. 2020). ISSN: 23993642. DOI: 10.1038/s42003-020-01300-w.

[13] Lianne Weber. *FREQUENCY ACTUATION OF DIFFERENT CONCENTRATIONS IRONSPERM IN IN VITRO SITUATION*. Tech. rep. University of Twente, 2023.

[14] Nafiseh Ebrahimi et al. *Magnetic Actuation Methods in Bio/Soft Robotics*. Mar. 2021. DOI: 10.1002/adfm.202005137.

[15] Mina M. Micheal et al. "2D Magnetic Actuation and Localization of a Surface Milli-Roller in Low Reynolds Numbers". In: *IEEE Robotics and Automation Letters* 7.2 (Apr. 2022), pp. 3874–3881. ISSN: 23773766. DOI: 10.1109/LRA.2022.3148787.

[16] Sylvain Martel and Mahmood Mohammadi. "Using a swarm of self-propelled natural microrobots in the form of flagellated bacteria to perform complex micro-assembly tasks". In: *Proceedings - IEEE International Conference on Robotics and Automation*. 2010, pp. 500–505. ISBN: 9781424450381. DOI: 10.1109/ROBOT.2010.5509752.

[17] Veronika Magdanz et al. *Sperm Cell Empowerment: X-Ray-Guided Magnetic Fields for Enhanced Actuation and Localization of Cytocompatible Biohybrid Microrobots*. Tech. rep.

[18] RadboudUMC. *Groeistoornis: 'grote' lengte*. 2023. URL: https://www.radboudumc.nl/patientenzorg/aandoeningen/groeistoornis.

[19] R J M Braks. *Motion control of IRONSperm clusters in a vascular model*. Tech. rep. University of Twente, 2023.

[20] Richard Spiegel. "Cobots Offer Advantages for Biomedical Testing Applications". In: *Medical Design Briefs* (Sept. 2022). URL: https://www.medicaldesignbriefs.com/component/content/article/46449-cobots-offer-advantages-for-biomedical-testing-applications#.

[21] Ugur Bozuyuk, Hakancan Ozturk, and Metin Sitti. "Microrobotic Locomotion in Blood Vessels: A Computational Study on the Performance of Surface Microrollers in the Cardiovascular System". In: *Advanced Intelligent Systems* 5.9 (Sept. 2023). ISSN: 26404567. DOI: 10.1002/aisy.202300099.

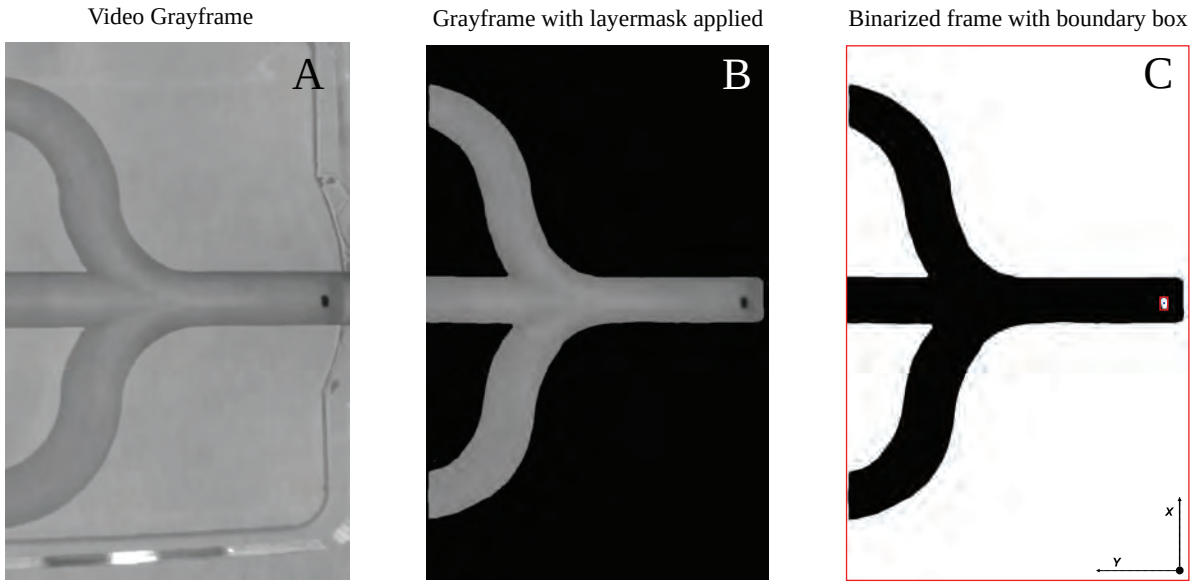

Fig. 14. **Visualization of the video processing to obtain the cluster position over time. A** Original video frame captured with the FLIR Backfly camera and gray scaled. **B** Layermask applied to the gray scaled image. **C** Binary frame with the layermask inverted and the value of the surroundings converted to 0. Every object above a manually chosen color threshold and pixel size will be detected, in this case the IRONSperm cluster, and shown as a white blob with a red boundary box and blue dot depicting the centroid position. The centroid position is tracked over time for each frame and the data is then stored.

VI. APPENDIX

A. *MATLAB Cluster Tracking script*

The video recordings of the experiments in this research were analyzed using a MATLAB script designed to track the cluster's position over time. The script processes the recordings frame by frame, cropping and rotating them to retain only the necessary information. Next, the video is gray scaled, as shown in Figure 14A, and converted to black and white using a manually selected threshold. This ensures that only the cluster is visible in black, with the background removed. The frame is then binarized and inverted, making the cluster appear white against a black background. If parts of the background are still not filtered out correctly, a layermask can be applied, setting the value of specific frame regions to 0 (Figure 14B). The 'regionprops' MATLAB function identifies binary white areas, extracting the right and left boundaries of the cluster, along with its centroid position (Figure 14C). This information is determined for each video frame and saved. Subsequently, the data can be retrieved and interpolated in order to visualize or plot it.

```
%% Choose which actions you want to enable (1 = enable, 0 = disable).
cropVid                 = 0;    % Crop and rotate the videoframes.
maskVid                 = 0;    % Used to filter out background noise in the videos.
                                % Only used for Experiment 2&3.
plotVid                 = 0;    % Plot the video to check whether the cluster is
                                % tracked correctly.
heightCheck             = 0;    % Check for loss of magnetic coupling.
                                % Only used for Experiment 1

%% Adjust these values as needed to enhance the contrast between the object and the
   background.
manualThreshold         = 120;  % Minimum color threshold of the object to track.
smallRegions            = 30;   % Minimum pixel size of the object to track.
                                % Filters out small regions, like cluster particles
                                   that break off.

% Get all video paths in one folder.
[vidPathNames, folderPathName] = getPathNames(cropVid);
```

```
for i = 1:length(vidPathNames)

    % Define current path and obtain the video object.
    vidPathName     = fullfile(folderPathName, vidPathNames{i});
    vidObj          = SelectVideo(vidPathName);


    % Crop the video.
    if cropVid == 1
        croppedVideoFile  = cropVideo(vidObj, folderPathName, vidPathNames{i});
    else
        croppedVideoFile = fullfile(folderPathName, vidPathNames{i});
    end



    % Process (&plot) the video and find the position data.
    [centroidHistory, firstFrame, lastFrame] = processVideo(croppedVideoFile,
       plotVid, maskVid, heightCheck, manualThreshold, smallRegions);


    saveName = vidPathNames{i};
    saveName = strrep(saveName, '.avi', '');
    saveName = strrep(saveName, '.mp4', '');
    saveName = append('M', saveName);

    saveData.(saveName).centroidHistory   = centroidHistory;
    saveData.(saveName).firstFrame        = firstFrame;
    saveData.(saveName).lastFrame         = lastFrame;


end


save("DataName.mat", '-struct', 'saveData');
disp('Data saved in struct, wohoo!')




function [pathNames, folderPathName] = getPathNames(cropVid)
%% Allow the user to select a video file by hand
    % folderPathName = uigetdir();

    if isequal(folderPathName,0)
        disp('User canceled the operation. Exiting the script.');
        return;
    end

    if cropVid == 1
        fileObj = dir(fullfile(folderPathName, '*.avi'));
    else
        fileObj = dir(fullfile(folderPathName, '*.mp4'));
    end
```

```
    nrOfFiles   = length(fileObj);
    pathNames   = cell(nrOfFiles,1);

    for i = 1:nrOfFiles
        pathNames{i} = fileObj(i).name;
    end

end



function vidObj = SelectVideo(vidPathName)
    vidObj = VideoReader(vidPathName);
end


function outputVideoFile = cropVideo(vidObj, folderPathName, vidPathNames)

    %% Adjust the ROI and rotation angle to your needs:

        % Specify the region of interest (ROI) for cropping [x, y, width, height]
        roi = [0, 0, 0, 0];


        % Set rotation angle (in degrees)
        rotationAngle = 0;



    % Create a VideoWriter object for the new video.
    outputVideoFile             = fullfile(folderPathName, ['cropped' vidPathNames])
       ;
    outputVideoFile             = strrep(outputVideoFile,'.avi','');
    outputVideoFile             = append(outputVideoFile, '.mp4');
    croppedVideoFile            = VideoWriter(outputVideoFile, 'MPEG-4');
    croppedVideoFile.FrameRate  = vidObj.FrameRate;
    croppedVideoFile.Quality    = 100;


    % Loop through the frames, crop, and write them to the new video.
    open(croppedVideoFile);

    while hasFrame(vidObj)
        frame        = readFrame(vidObj);
        rotatedFrame = imrotate(frame, rotationAngle);
        croppedFrame = imcrop(rotatedFrame, roi);
        writeVideo(croppedVideoFile, croppedFrame);
    end


    % Close the VideoWriter object.
    close(croppedVideoFile);

    disp(['Video ' vidPathNames ' processed and saved as cropped' outputVideoFile]);

end
```

```
function [centroidHistory, firstFrame, lastFrame] = processVideo(croppedVideoFile,
    plotVid, maskVid, heightCheck, manualThreshold, smallRegions)

    % Initializing variables
    i           = 0;
    firstFrame  = 0;
    lastFrame   = 0;

    croppedVideo        = VideoReader(croppedVideoFile);
    centroidHistory     = NaN(croppedVideo.NumFrames, 7);
    boundaryHistory     = NaN(croppedVideo.NumFrames, 7);


    % OPTIONAL: Apply a binary layer mask. Insert the black and white images you
       want to use as a layermask.
    if maskVid == 1
        LayerMask       = imread('ImageName.png');
        grayLayerMask   = rgb2gray(LayerMask);
        binaryMask      = imbinarize(grayLayerMask);
        binaryMask      = imcomplement(binaryMask);
    end

    while hasFrame(croppedVideo)
        %% Video processing
        i = i + 1;  % Frame counter

        % Read a frame.
        frame = readFrame(croppedVideo);

        % Convert the frame to grayscale.
        grayFrame = rgb2gray(frame);

        % Overlay the layermask.
        if maskVid ~= 0
            grayFrameMasked(binaryMask) = 0;
        else
            grayFrameMasked = grayFrame;
        end


        % Binarize the frame using the manual threshold.
        binaryFrame = grayFrameMaskedContrasted < manualThreshold;

        % Filter out small regions / noise removal.
        binaryFrame = bwareaopen(binaryFrame, smallRegions);



    %% Find boundaries and centroid of the sample.

        % Finding the centroid position ONLY if the object is in frame
        stats       = regionprops(binaryFrame, 'BoundingBox', 'Centroid');
        emptyStats  = isempty(stats);

        if (~isempty(stats))
```

```
    if (firstFrame == 0)
        firstFrame = i; % Store the number of the first frame where the
           cluster is visible.
    end

    % boundaries = stats.BoundingBox;
    % centroid = stats.Centroid;

    % % Store the centroid position in the cell array.
    centroidHistory(i,1)  = i;                  % framenumber
    centroidHistory(i, 2) = centroid(1,1);      % X-position [px]
    centroidHistory(i, 3) = centroid(1,2);      % Y-position [px]

    boundaryHistory(i,1)  = i;                  % framenumber
    boundaryHistory(i, 2) = boundaries(1,1);    % X-position [px]
    boundaryHistory(i, 3) = boundaries(1,2);    % Y-position [px]

    end




    % Stop the video processing when the sample loses magnetic coupling and
       falls.
    if heightCheck == 1
        initialHeight   = centroidHistory(firstFrame, 3);
        currentHeight   = centroidHistory(i, 3);
        heightfall      = abs(initialHeight - currentHeight);

        if heightfall > 120
            disp('The sample can''t keep up with the RPM.')
            lastFrame = i;
            break;
        end
    end


else
    if ((firstFrame ~= 0) && (lastFrame == 0))
                lastFrame = i;
    end

end



%% Video plotting
if plotVid == 1
        figure(1), clf
        sgtitle('Visualization of the experiment video processing')

        % Display the original video.
        subplot(1, 3, 1)
        imshow(grayFrame);
        title('Grayframe')
        ylabel('y');
```

```
                % Show the gray frame video with layermask applied.
                subplot(1, 3, 2)
                imshow(grayFrameMasked);
                title('Grayframe with layermask applied')

                % Display the original binary image with bounding boxes.
                subplot(1, 3, 3)
                ylabel('y');
                imshow(binaryFrame);
                title('Binarized frame with boundary box');
                hold on;

                % Loop through each region and plot the bounding box.
                for k = 1:length(stats)
                    rectangle('Position', stats(k).BoundingBox, 'EdgeColor', 'r', '
                       LineWidth', 0.5);
                end

            if (~emptyStats)
                % Plot the centroid in red on the binary frame.
                plot(centroid(1,1), centroid(1, 2), 'b.', 'LineWidth', 3);
                hold off;

                % Pause to visualize each frame.
                pause(1/croppedVideo.FrameRate);

            end
        end
    end
end
```

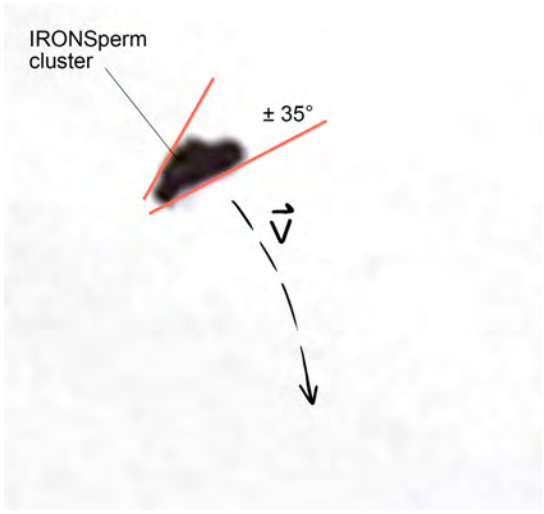

Fig. 15. Image of the cluster's cone shape as observed during Experiment 2.

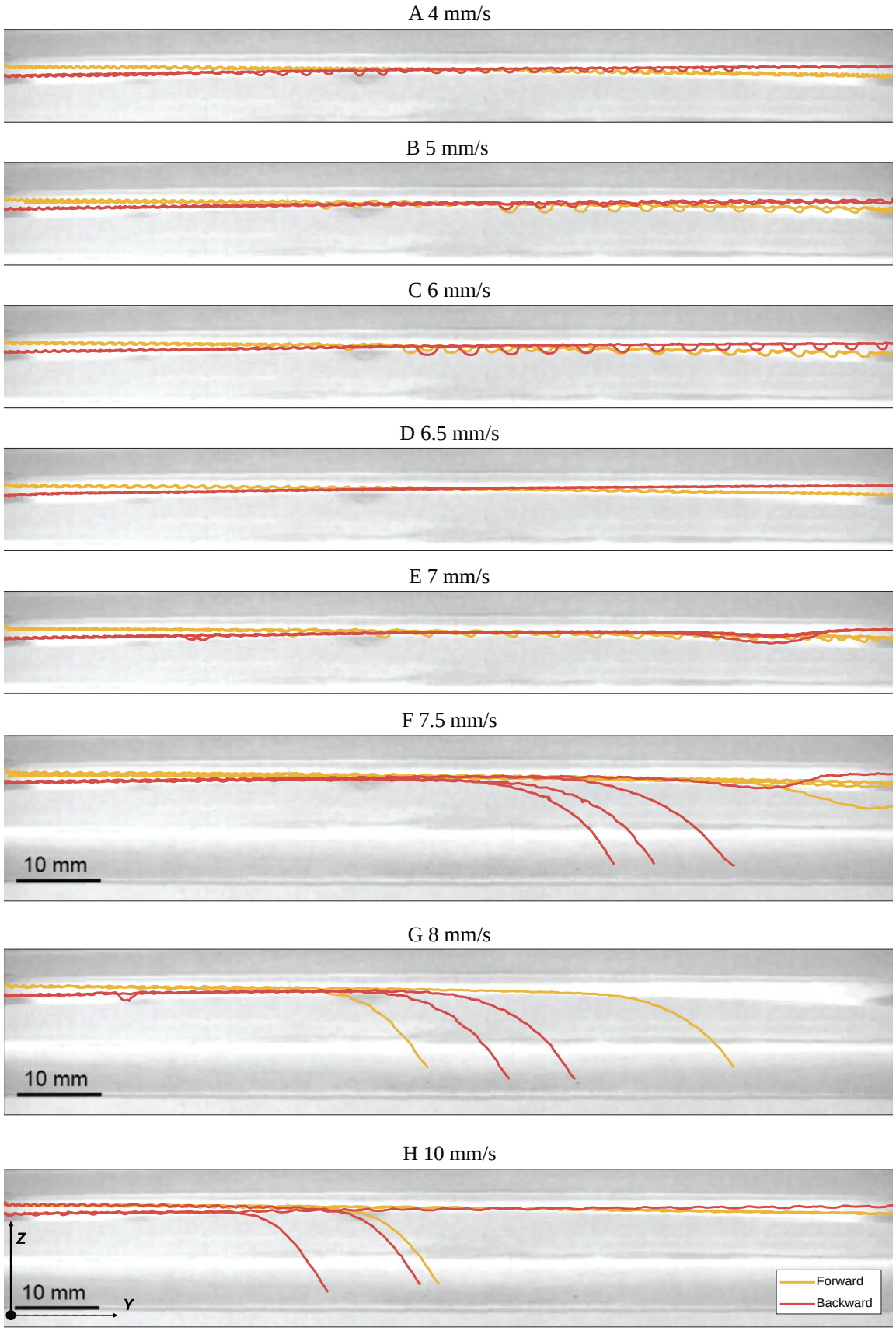

Fig. 16. Position of the IRONSperm cluster inside of the acrylic tube. Forward movement is depicted by the yellow lines. Backwards movements are plotted in reverse and are depicted by the red lines. The rolling locomotion of the cluster is easily discernible through the sinusoidal shapes evident in the plot.

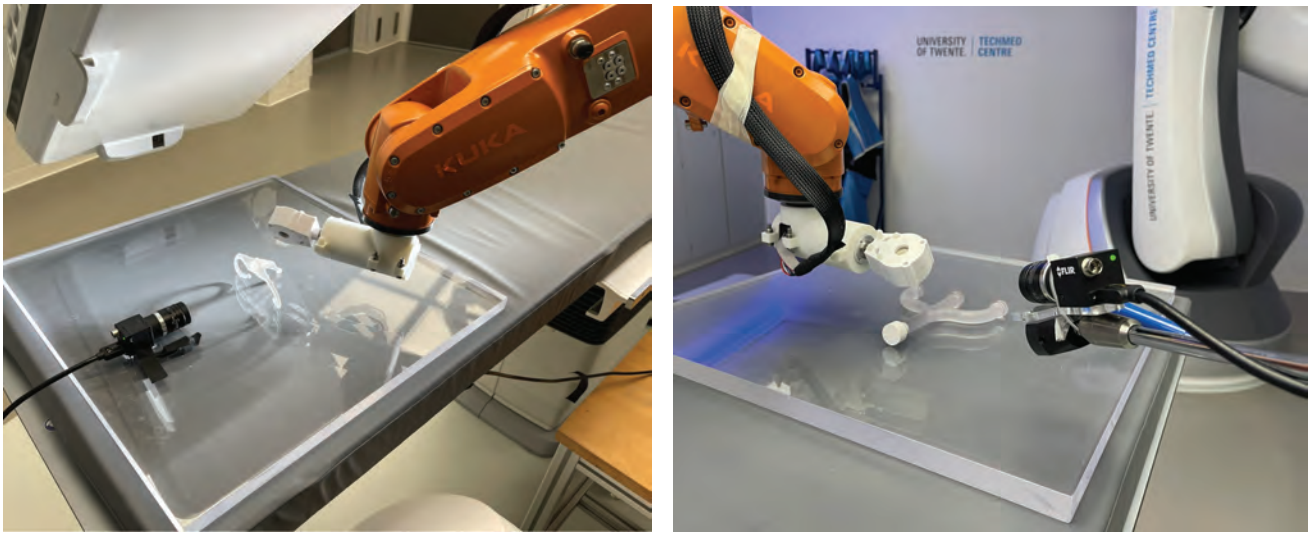

Fig. 17. Experimental X-ray set-up while imaging the cluster inside the uterus and trifurcation phantom.

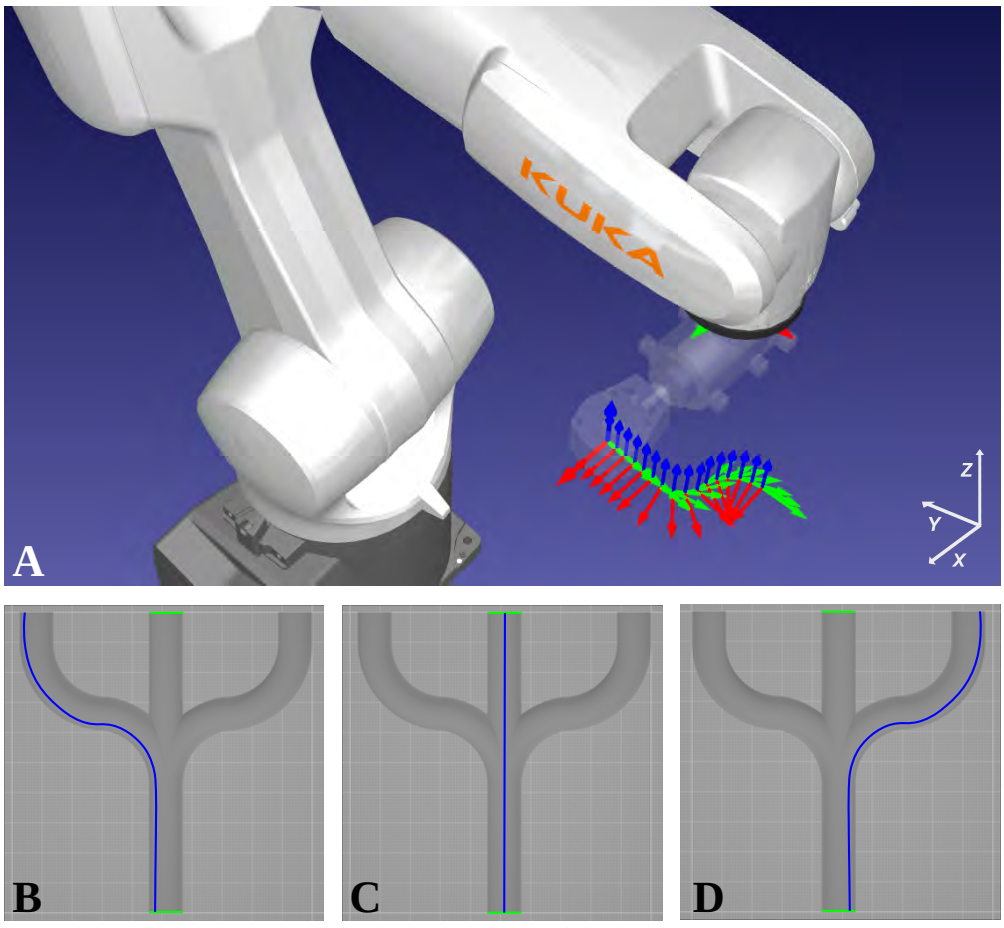

Fig. 18. Visualization of the left, straight and right trajectory drawing and the translation of the drawn paths to the program RoboDK